Nucleon-Nucleus Optical-Model Parameters, $A > 40$, $E < 50$ MeV*

F. D. Becchetti, Jr., and G. W. Greenlees

School of Physics, University of Minnesota, Minneapolis, Minnesota 55455

(Received 30 December 1968)

Proton-nucleus and neutron-nucleus standard optical-model parameters are given that represent, quite well, much of the elastic scattering data in the range $A > 40$, $E < 50$ MeV. These parameters were determined by fitting simultaneously a large sample of the available proton data, and independently, a large sample of the available neutron data. Explicit energy- and isospin-dependent terms were included and their coefficients obtained directly from the data analysis. The results are shown to be consistent with the range and strength of the central and isospin components of the two-body interaction.

I. INTRODUCTION

IN recent years, accurate elastic scattering data for protons on medium to heavy weight nuclei have appeared. In many instances, polarization and reaction cross-section data have been measured also at the same energies and using isotopically separated targets. Together with older proton and neutron data, mostly using natural targets, a substantial amount of nucleon-nucleus scattering information now exists. Many of these data have been analyzed individually in terms of the standard nuclear optical model (OM)[1–5] and in several instances the individual parameters have been used to extract some information about the energy and isospin dependence of the OM potentials. However, because of the inherent potential ambiguities, the parameters found by various authors differ somewhat and make interpolation between different energies and nuclei uncertain. In a distorted-wave Born-approximation (DWBA) or coupled-channels analysis, then, one often does not have reliable OM parameters for the nucleon elastic channels.

Besides the obvious utilitarian value of such parameters, there is reason to believe that useful information about nuclear forces and nuclear structure can be obtained from the systematic analysis of nucleon elastic scattering.

In view of the amount of data available and the inherent parameter ambiguities in the OM potentials, it is clearly impractical to analyze individual data sets and hope to determine an optimum general parameter set. The obvious approach is to combine a large number of individual data taken over a range of energies and nuclei, include explicit energy, isospin, etc., terms as variable parameters in the OM potentials and fit simultaneously all of the data. Such an analysis is well within the capabilities of computers presently available and is presented here.

II. OPTICAL-MODEL PROGRAM

A FORTRAN IV OM code[6] was written by one of the authors (FDB) to solve the appropriate time-independent nonrelativistic local Schrödinger equation for the partial-wave scattering amplitudes. This code used a modified numerov method[7] and included an automatic least-squares search routine which could optimize up to 30 parameters. Using a 60K 60-bit word CDC 6600 computer, this program could fit simultaneously 46 data sets with each data set consisting of up to 90 differential cross-section points, 90 polarization points, and either the total cross section (neutrons) or the reaction cross section (protons).

In order to minimize the computation time and the storage requirements, the experimental data were interpolated to the nearest even c.m. angles. This allows many of the angle-dependent functions to be prestored in single common arrays. Also, many of the proton data [30 MeV $\sigma(\theta)$] were measured at even c.m. angles and at least half the other data points (due to the lab-c.m. transformation) were within 0.2° of even c.m. angles, so that a majority of the data points required little, if any, interpolation. Several checks were made using 40-MeV data to insure that only negligible errors were introduced in this procedure.

The criterion function F of the theoretical fit was taken to be

$$F = \sum_{n=1}^{n_{max}} \left[\frac{\chi^2}{N_{\sigma(\theta)}} + \frac{\chi^2}{N_{P(\theta)}} + \chi^2_{\sigma_R} \right]_n, \qquad (1)$$

where:

$\chi^2/N_{\sigma(\theta)} =$ the χ^2 per point value of the differential cross sections $\sigma(\theta)$ for the nth data set ($n \leq 46$);

$\chi^2/N_{P(\theta)} =$ the χ^2 per point value of the polarization data $P(\theta)$ for the nth data set;

and

$\chi^2_{\sigma_R} =$ the χ^2 value of the reaction (protons) or total (neutrons) cross section for the nth data set.

[1] F. G. Perey, Phys. Rev. 131, 745 (1963).
[2] L. Rosen, J. G. Beery, A. S. Goldhaber, and E. H. Auerbach, Ann. Phys. (N.Y.) 34, 96 (1965).
[3] G. R. Satchler, Nucl. Phys. 92, 273 (1967).
[4] M. P. Fricke, E. E. Gross, B. J. Morton, and A. Zucker, Phys. Rev. 156, 1207 (1967).
[5] G. W. Greenlees and G. J. Pyle, Phys. Rev. 149, 836 (1966).
[6] F. D. Becchetti, Jr., M.S. thesis, University of Minnesota, 1968 (unpublished).
[7] M. A. Melkanoff, T. Sawada, and J. Raynal, in *Methods in Computational Physics*, edited by B. Alder (Academic Press Inc., New York, 1966), Vol. VI, p. 1.

A quantity $\chi^2/N_{g(\theta)}$ is defined by

$$\frac{1}{N} \sum_N \left(\frac{g^{OM}(\theta) - g^{obs}(\theta)}{\Delta g^{obs}(\theta)} \right)^2, \qquad (2)$$

where $g^{OM}(\theta)$, $g^{obs}(\theta)$, and $\Delta g^{obs}(\theta)$ are the OM prediction of $g(\theta)$, the interpolated experimental value, and the standard deviation error in $g(\theta)$, respectively, for the N even c.m. angles. It should be noted that, unlike most OM analyses F [as defined by Eq. (1)] adds the χ^2 per point values rather than the χ^2 values. The present definition does not, then, treat all data points equivalently. The reason for this choice of F is given below.

The OM potentials, through the asymptotic form of the OM wave functions, represent, indirectly, the scattering matrix (S matrix) comprised of the complex phase shifts. The S matrix in turn determines the ordinary scattering amplitude $A(\theta)$ and the spin-flip amplitude $B(\theta)$. The measured quantities $P(\theta)$ and $\sigma(\theta)$ are related to these by[7,8]

$$\sigma(\theta) = |A(\theta)|^2 + |B(\theta)|^2$$

and

$$P(\theta) = 2Im A^*(\theta) B(\theta)/\sigma(\theta). \qquad (3)$$

When the spin-orbit interaction is small, $|B(\theta)| \ll |A(\theta)|$ and $\sigma(\theta)$ is determined primarily by $A(\theta)$. Thus, in order to determine both amplitudes accurately, $P(\theta)$ and $\sigma(\theta)$ must be weighted equally.

A typical set of proton experimental data at a single energy for a single nucleus includes 30–90 $\sigma(\theta)$ points of accuracy ± 3–10%, 10–40 $P(\theta)$ points of accuracy ± 10–30%, and possibly, the reaction cross section. Using a criterion function defined by summing χ^2 values for each point would weight the cross-section points considerably more than the $P(\theta)$ and σ_R points. This effect is emphasized in the case of the $P(\theta)$ points where the experimental and predicted values are bounded between ± 1.0; this limits χ^2 for the polarization points to values (<50, in general for typical experimental errors) which are several orders of magnitude lower than the possible values of χ^2 for the $\sigma(\theta)$ and σ_R points. An analysis based upon minimizing the simple sum of χ^2 values can thus weight, almost entirely, the $\sigma(\theta)$ data and determine primarily the quantity $A(\theta)$. In such circumstances, the spin-orbit potential is being used to fit the large angle $\sigma(\theta)$ points at the expense of the over-all fit to the $P(\theta)$ and σ_R data. It then becomes very difficult to extract useful information about either the spin-orbit or the central potentials, or to have confidence in the scattering amplitudes and wave functions determined by such potentials. The criterion function, as presently defined F [Eq. (1)], is thus purposely constructed to weight equally the three observables: $\sigma(\theta)$, $P(\theta)$, and σ_R (or σ_T). Such a procedure does not avoid the difficulties arising from $P(\theta)$ being bounded

between ± 1. However, such difficulties are unimportant if comparable χ^2 values are achieved for the various individual experimental points, as is the case here. This procedure also tends to over emphasize the σ_R (or σ_T) measurements. In practice, considerably fewer proton σ_R measurements are available than $\sigma(\theta)$ and $P(\theta)$ angular distributions and the contribution of the σ_R points to F is thus reduced. A corresponding situation does not hold for the neutron data where many σ_T values are available. However, in practice, there were insufficient neutron data available to enable a completely independent neutron analysis to be made and the proton results were used as a guide to suitable parameterizations to be tried.

The OM predictions used in calculating F included several corrections in order to make them directly comparable to experimental data. Both the $\sigma(\theta)$ and $P(\theta)$ predictions are obtained by averaging the OM values over a rectangular detector aperture of width $\Delta\theta$ equivalent to the experimental detector geometry.[9] This correction is necessary for most of the polarization data since $\Delta\theta$ is usually several degrees. Provisions were also available for including isotropic compound elastic scattering. This correction, which was assumed to be unpolarized, was determined using an analytic expression to minimize χ^2 for the individual $\sigma(\theta)$ data sets. The expressions for $\sigma(\theta)$, $P(\theta)$, and σ_R or σ_T then become

$$\sigma(\theta) = \sigma'(\theta) + \sigma_{CE}(\theta), \qquad \text{differential cross section}$$

$$P(\theta) = P'(\theta) \left[\frac{\sigma'(\theta)}{\sigma'(\theta) + \sigma_{CE}(\theta)} \right],$$

polarization

$$\sigma_R = \sigma_R' - \sigma_{CE}, \qquad \text{reaction cross section} \qquad (4)$$
$$\sigma_E = \sigma_E' + \sigma_{CE}, \qquad \text{elastic cross section}$$
$$\sigma_T = \sigma_T', \qquad \text{total cross section}$$

where $\sigma_{CE}(\theta) = \sigma_{CE}/4\pi$ is the optimum isotropic compound elastic scattering correction to minimize χ^2 for $\sigma(\theta)$, and $\sigma'(\theta)$, $P'(\theta)$, etc., are the OM values corrected only for the finite detector width. At low energies ($E < 10$ MeV), the compound elastic correction can become significant, and this, of course, must be taken into consideration when selecting experimental data for analysis.

Finally, the experimental errors used in calculating χ^2 for $\sigma(\theta)$ are the quoted statistical errors in standard deviations. Systematic errors in $\sigma(\theta)$ were included by allowing renormalization of the experimental points. The renormalization constant was chosen to minimize χ^2 and was constrained to be within the experimental renormalization error. Data which also included compound elastic corrections were renormalized using only the forward angle $(\theta < 60°)$ $\sigma(\theta)$ data since for most of these points $\sigma(\theta) \gg \sigma_{CE}/4\pi$.

[8] P. E. Hodgson, in *The Optical Model of Elastic Scattering* (Oxford University Press, London, 1963), Chap. 2.

[9] C. Poppe and G. J. Pyle, University of Minnesota, J. H. Williams Laboratory Annual Progress Report, p. 125, 1965 (unpublished).

The optimum parameters were then determined by minimizing the F function calculated using the corrected OM predictions given by (4).

III. SELECTION OF EXPERIMENTAL DATA

Proton Data

The selection of the experimental proton data to be analyzed was determined by several factors, the primary ones being accuracy and completeness, i.e., that the data usually include not only $\sigma(\theta)$ measurements but also $P(\theta)$ and σ_R data. It was also essential that the data span a wide range of nonrelativistic energies and include substantial variations in N and Z. Since the data analyzed should be predominantly non-Coulomb direct shape-elastic scattering data, the lowest incident energy included was determined primarily by the appropriate Coulomb barrier (approximately 7–12 MeV) and the (p, n) threshold Q values (2–10 MeV). The limits on the incident proton energies were thus determined to be $10 < E < 100$ MeV.

Using these criteria, 46 proton data sets (a single data set includes all elastic scattering information for one nucleus at a single energy) were selected from the data available. These data are concentrated at proton energies of 10, 14.5, 30, and 40 MeV and are representative of the most accurate data available. The distribution with E and $(N-Z)/A$, of proton data sets analyzed, is shown in Fig. 1 (see Refs. 10–32). All of the proton OM parameters were determined by simultaneously fitting these data.

Included in the 46 data sets are 40 $\sigma(\theta)$, 28 $P(\theta)$, and 8 σ_R measurements comprising about 2500 data points. Typical $\sigma(\theta)$ data are of accuracy ± 3–$\pm 15\%$ with $\pm 5\%$ renormalization errors and cover the angular range $15°$ $(2.5°)$–$160°$ with a detector acceptance $0.2°$. Typical $P(\theta)$ data are of accuracy ± 0.02–± 0.2 absolute, with $\theta = 15°$ $(5°)$–$120°$ and a detector acceptance of $1°$–$4°$. The σ_R data are typically $\pm 5\%$. Wherever possible statistical and renormalization errors have been separated and included as standard deviations. The data weight most heavily the $\sigma(\theta)$ and $P(\theta)$ measurements for nuclei $A < 90$ and energies > 10 MeV. Most of the target nuclei have net spin $I = 0$ and a first excited state which is energetically well separated from the ground state.

Light nuclei $(A < 40)$ were not included since these tend to exhibit considerable level structure at the energies involved here. They also have $N \approx Z$ and would yield little information about the OM isospin terms which depend on the neutron excess.

Additional proton data which became available at various stages of the analysis were used as an independent check of the final parameter sets.

Neutron Data

Because of the inherent experimental difficulties, the relative accuracy and quantity of the available neutron elastic scattering data is substantially less than that for protons. Most of the published data for neutrons are at energies below 24 MeV from natural targets and seldom include polarization results. Of the data available, 30 data sets were selected for analysis. These include 30 $\sigma(\theta)$, 4 $P(\theta)$, and 28 σ_T measurements consisting of 1000 points of accuracy ± 10–$\pm 30\%$ over the range $\theta = 10°(5°)$–$160°$ with a detector acceptance of $1°$–$5°$. The nuclei and energies included in the analysis are shown in Fig. 2 (see Refs. 33–39). Where natural targets had been used, Fig. 2 uses the weighted average of $(N-Z)/A$ among the isotopes.

These data consist mostly of $\sigma(\theta)$ and σ_T data for natural targets $A > 90$ and energies $E < 14.5$ MeV. Generally, the nuclei and energies are quite different from those covered by the proton data. Also, since much of the data are at energies below 10 MeV, substantial compound elastic corrections were often included.

The neutron data were used primarily as a check of features revealed by the proton data.

[10] L. Lee, Jr., and J. P. Schiffer, Phys. Rev. **134**, B765 (1964).

[11] P. J. Bulman, G. W. Greenlees, and M. J. Sametband, Nucl. Phys. **69**, 536 (1965).

[12] G. Igo and B. D. Wilkens, Phys. Letters **2**, 342 (1962).

[13] R. D. Albert and L. F. Hansen, Phys. Rev. Letters **6**, 13 (1961).

[14] V. Meyer and N. M. Hintz, Phys. Rev. Letters **5**, 207 (1960).

[15] I. F. Dicello, G. J. Igo, and M. L. Roush, Phys. Rev. **157**, 1001 (1967).

[16] J. F. Turner, B. W. Ridley, P. F. Cavanagh, G. A. Gard, and A. G. Hardacre, Nucl. Phys. **58**, 509 (1964).

[17] G. W. Greenlees, U. Haznedaroglu, A. B. Robbins, P. M. Rolph, and J. Rosenblatt, Nucl. Phys. **49**, 496 (1963).

[18] J. Benveniste, A. C. Mitchell, B. Buck, and C. B. Fulmer, Phys. Rev. **133**, B323 (1964).

[19] J. E. Durisch, R. R. Johnson, and N. M. Hintz, Phys. Rev. **137**, B904 (1965).

[20] See Ref. 17.

[21] See Ref. 2.

[22] D. A. Lind et al. (to be published).

[23] J. E. Dayton and G. Schrank, Phys. Rev. **101**, 1358 (1956).

[24] D. J. Baugh, G. W. Greenlees, J. S. Lilley, and S. Roman, Nucl. Phys. **65**, 33 (1965).

[25] C. B. Fulmer, Phys. Rev. **125**, 631 (1962).

[26] J. B. Ball, C. B. Fulmer, and R. H. Bassel, Phys. Rev. **135**, B706 (1964).

[27] B. W. Ridley and J. F. Turner, Nucl. Phys. **58**, 497 (1964).

[28] R. M. Craig, J. C. Dore, G. W. Greenlees, J. S. Lilley, J. Lowe, and P. C. Rowe, Nucl. Phys. **58**, 515 (1964).

[29] D. L. Watson, J. Lowe, J. C. Dore, R. M. Craig, and D. J. Baugh, Nucl. Phys. **A92**, 193 (1967).

[30] See Ref. 4.

[31] H. Liers, M. S. thesis, University of Minnesota, 1967 (unpublished).

[32] C. F. Hwang, G. Clusnitzer, D. H. Nordby, S. Suwa, and J. H. Williams, Phys. Rev. **131**, 2602 (1963).

[33] Data compiled in University of California Radiation Laboratory Report No. UCRL 5351, 1958 (unpublished).

[34] Y. V. Dukarevich, A. N. Dyumin, and D. M. Kaminker, Nucl. Phys. **A92**, 433 (1967).

[35] J. R. Beyster, M. Walt, and E. W. Salmi, Phys. Rev. **104**, 1319 (1956).

[36] Compilation of data by F. Bjorklund, S. Fernbach, and W. Sherman, Phys. Rev. **101**, 1832 (1956).

[37] J. H. Coon, R. W. Davis, H. E. Felthauser, and D. B. Nicodemus, Phys. Rev. **111**, 250 (1958).

[38] T. P. Stuart, J. D. Anderson, and C. Wong, Phys. Rev. **125**, 276 (1962).

[39] C. Wong, J. D. Anderson, J. W. McClure, and B. D. Walker, Phys. Rev. **128**, 2339 (1962).

IV. DATA ANALYSIS

Optical Potential

The optical potential $V(r)+iW(r)$, which was used is a combination of Woods-Saxon volume and surface derivative, forms with

$$V(r) = -V_R f(r, R_R, a_R) \qquad \text{central real}$$

$$+V_{so}\mathfrak{d}\cdot\mathbf{l}\lambda_\pi^2(1/r)\,(d/dr)\big[f(r, R_{so}, a_{so})\big]$$

$$\text{spin-orbit}$$

$$+(Zze^2/2R_c)\big[3-(r^2/R_c^2)\big]$$

$$\text{for } r \leq R_c \text{ Coulomb}$$

$$+Zze^2/r \qquad \text{for } r \geq R_c, \text{ Coulomb} \quad (5)$$

and

$$W(r) = -W_v f(r, R_I{}', a_I{}'), \qquad \text{imaginary volume}$$

$$= +W_{SF}4a_I(d/dr)\big[f(r, R_I, a_I)\big],$$

$$\text{imaginary surface,}$$

where

$$f(r, R, a) = [1+\exp(r-R)/a]^{-1}.$$

$\mathfrak{d}\cdot\mathbf{l}$ = scalar product of the intrinsic and orbital angular momentum operators

$$= l \text{ for } j = l + \tfrac{1}{2}$$

$$= -(l+1) \text{ for } j = l - \tfrac{1}{2} > 0.$$

j, l = total and orbital angular momentum quantum numbers for the incident nucleon (spin, $s=\tfrac{1}{2}$).

λ_π^2 = pion Compton wavelength squared $\approx 2.0 \text{ F}^2$.

Z, z = target and incident particle charge.

A = target mass number.

Energies in MeV, lengths in fermis ($1\text{ F} = 10^{-13}$ cm).
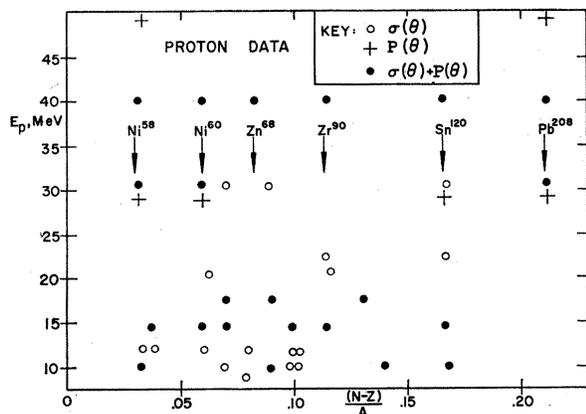
FIG. 1. The energy and $(N-Z)/A$ values of the proton data included in the parameter searches. The data are taken from Refs. 10–32.
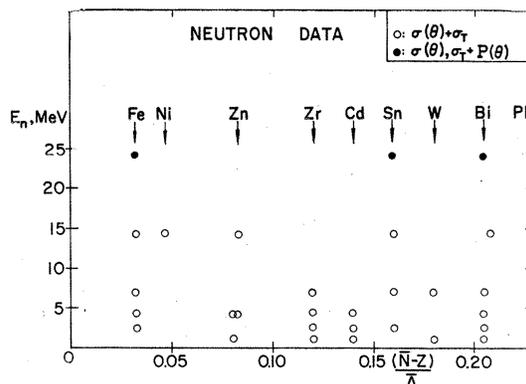
FIG. 2. The energy and average $(N-Z)/A$ values of the neutron data included in the parameter searches. The data is taken from Refs. 33–39.

The Coulomb potential is one due to a uniformly charged sphere of total charge Ze and radius R_c. This potential can be shown to give the same electron and proton scattering cross sections as a more realistic electrostatic potential calculated from the empirical nuclear charge distribution, provided the rms radii are made equal.[40] Unless otherwise noted the semiempirical formula given by Elton was used to calculate R_c.[41]

It is customary to assume an $A^{1/3}$ variation for all the radii, i.e., $R_R = r_R A^{1/3}$, etc. This assumption about the geometry of the potentials is certainly only an approximation and, as such, complicates the interpretation of the A, Z, or N dependence of the other parameters. However, in lieu of a better approximation, the radii were taken, initially to have the form

$$R_R = r_R A^{1/3},$$

$$R_{so} = r_{so} A^{1/3},$$

$$R_c = r_c A^{1/3},$$

$$R_I{}' = r_I{}' A^{1/3},$$

$$R_I = r_I A^{1/3}.$$

The strength and geometry of the optical potential is thus determined by V_R, r_R, a_R; V_{so}, r_{so}, a_{so}; W_v, $r_I{}'$, $a_I{}'$; W_{SF}, r_I, a_I. These quantities were further parameterized in terms of A, Z, N, and E as required to fit the data.

Parameter Search

Since the proton-nucleus data are substantially more accurate and cover a wider range of energies and nuclei than the neutron data, the main emphasis was necessarily directed towards fitting the proton data. The general scheme followed was to optimize first the OM

[40] F. D. Becchetti, Jr., and G. W. Greenlees, University of Minnesota, J. H. Williams Laboratory Annual Progress Report, p. 115, 1965 (unpublished).

[41] L. R. B. Elton, in *Nuclear Sizes* (Oxford University Press, London, 1961), p. 36.
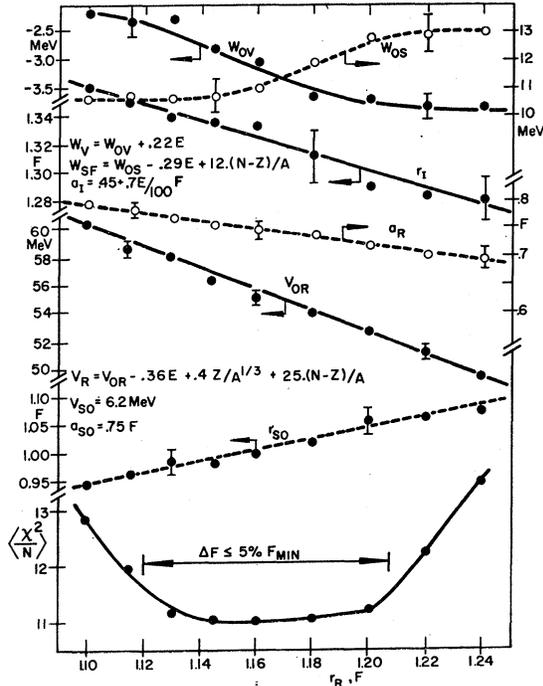
FIG. 3. Parameter correlations found in the proton analysis using the strength forms shown.

fit for protons using a particular form of parameterization and then modify the more successful forms, as necessary, to fit the neutron data. As a result, considerably fewer forms of neutron parameterization were investigated.

It is known from previous analyses that the OM predictions are most sensitive to the surface regions of the optical potentials. Usually several different combinations of strength and geometry parameters can be found that give nearly the same OM predictions.[1-5] The A, Z, N, or E dependence of the potentials can often be assigned to either the strength or the geometry. In the present analysis it was decided to parameterize, whenever possible, only the strength terms V_R, W_V, W_{SF}, and V_{so}.

Proton Parameters

The initial fit to the proton data was attempted using the form

$$V_R = V_{OR} + V_{ER}E + 0.4Z/A^{1/3} + V_{sym}(N-Z)/A,$$

$$W_V = W_{OV} + W_{EV}E,$$

$$W_{SF} = W_{OS} + W_{ES}E$$

with $r_I' = r_I$, $a_I' = a_I$. E is the incident lab energy. The term $0.4 Z/A^{1/3}$ is used to correct for Coulomb repulsion effects and is the value used by Perey.[1] Implicit in this value is an energy dependence for the nucleon real

potential strength of about $-0.3E$ and an average nuclear Coulomb energy of $1.38 Z/A^{1/3}$ MeV.[1]

Optimum parameters were obtained by performing a series of subsearches on groups of six parameters or less, chosen to avoid the more prominent strength-geometry parameter correlations. A range of geometrical parameters centered about the values $r_R = 1.2$, $a_R = 0.7$, $r_I = 1.3$, $a_I = 0.6$, $r_{so} = 1.1$, and $a_{so} = 0.7$ was investigated. The typical χ^2/N value obtained was about 20 per point.

The subsearches on W_{OS} indicated a mass dependence of the surface absorption. Different forms of W_{SF} were investigated with the best fit obtained using an $(N-Z)/A$ dependence (see Table I). Although a substantial improvement was affected ($\chi^2/N = 15$) the OM predictions for σ_R were consistently 10–20% higher than experimental values. In an attempt to improve the σ_R predictions various A- and E-dependent terms were included in W_V, r_I, and a_I. The most significant improvement was found by introducing a term proportional to $(N-Z)/A$ into a_I. As a general criterion, a uniform reduction in F of 20% or more was considered significant enough to include an additional parameter in the OM potential.

This latter form, with a_I having an $(N-Z)/A$ dependence, ultimately gave the best over-all fit to the 46 proton data sets. However, even when restricted to this form, several sets of parameters were found which give equivalent OM fits; these are listed in Table I. The parameter correlations found are shown in Fig. 3. Also V_{sym}, the $(N-Z)/A$ coefficient in V_R, depends upon the coefficient used for the $Z/A^{1/3}$ term, the Coulomb correction term.

These features, of course, must be taken into consideration when interpreting the parameters. Nonetheless, the optimum proton-nucleus standard OM parameters were determined to be

$$V_R = 54.0 - 0.32E + 0.4Z/A^{1/3} + 24.0(N-Z)/A,$$

$$r_R = 1.17, \quad a_R = 0.75,$$

$$W_V = 0.22E - 2.7, \quad \text{or zero, whichever is greater,}$$

$$W_{SF} = 11.8 - 0.25E + 12.0(N-Z)/A,$$

$$\text{or zero, whichever is greater,} \quad (8)$$

$$r_I = 1.32, \quad a_I = 0.51 + 0.7(N-Z)/A,$$

$$V_{so} = 6.2,$$

$$r_{so} = 1.01, \quad a_{so} = 0.75,$$

where $E =$ incident lab energy.

A listing is given in Table I of the different parameterizations investigated which yielded acceptable values for F. Average values of χ^2/N for each observable are given for comparison. These average values were obtained by calculating the mean of all the χ^2/N values of a particular quantity using the data sets included in the parameter search. The parameters of Table I

TABLE I. A listing of the parameters found in the analysis of the proton data of Fig. 1 using different potential forms. Only those forms giving reasonable fits to the data have been included.

Comments[a]	V_R (MeV)	r_R, a_R (F)	W_V (MeV)	W_{SF} (MeV)	r_I, a_I (F)	V_{so}, r_{so}, a_{so}	$\langle x^2/N \rangle$ $\sigma(\theta)$	$P(\theta)$	σ_R
Best fit	$54.-0.32E+0.4\gamma+24.\xi$	1.17, 0.75	$0.22E-2.7$	$11.8-0.25E+12.\xi$	$1.32, 0.51+0.7\xi$	6.2, 1.01, 0.75	12	7	6
Grid on r_R	(See Fig. 3 for parameters.)						14	9	10
a_I constant	$54.-0.32E+0.4\gamma+24.\xi$	1.17, 0.75	$0.22E-2.7$	$11.8-0.25E+12.\xi$	1.32, 0.56	6.2, 1.01, 0.75	16	8	6
$a_I\propto A^{1/4}, W_V\propto E$	$54.-0.32E+0.4\gamma+24.\xi$	1.17, 0.75	$0.15E$	$11.8-0.25E+12.\xi$	$1.32, 0.18A^{1/4}$	6.2, 1.01, 0.75	13	7	8
$a_I\propto A^{1/3}$	$54.-0.32E+0.4\gamma+24.\xi$	1.17, 0.75	$0.22E-2.7$	$11.8-0.25E+12.\xi$	$1.32, 0.14A^{1/3}$	6.2, 1.01, 0.75	12	7	8
$W_V\propto\xi$	$54.-0.32E+0.4\gamma+24.\xi$	1.17, 0.75	$0.22E-2.7+1.4\xi$	$11.8-0.25E+12.\xi$	1.32, 0.56	6.2, 1.01, 0.75	14	7	7
$W_{SF}\propto A^{2/3}$	$54.-0.32E+0.4\gamma+24.\xi$	1.17, 0.75	$0.22E-2.7$	$0.77A^{2/3}-0.28E$	$1.27, 0.51+0.7\xi$	6.2, 1.01, 0.75	20	9	10
$r_{so}=r_R=1.17$	$54.-0.32E+0.4\gamma+24.\xi$	1.17, 0.75	$0.22E-2.7$	$11.8-0.25E+12.\xi$	$1.32, 0.51+0.7\xi$	5.9, 1.17, 0.60	16	9	6
$V_{so}\propto E$	$54.-0.32E+0.4\gamma+24.\xi$	1.17, 0.75	$0.22E-2.7$	$11.8-0.25E+12.\xi$	$1.32, 0.51+0.7\xi$	$9.0-0.1E, 1.01, 0.75$	13	7	6
$V_R\propto E^2$	$59.7-0.47E+0.9E^2+0.4\gamma+24.\xi$	1.15, 0.76	$0.22E-2.7$	$11.8-0.25E+12.\xi$	$1.32, 0.51+0.7\xi$	6.2, 1.01, 0.75	17	8	7
Best $r_R=1.12$	$58.8-0.32E+0.4\gamma+24.\xi$	1.12, 0.78	$0.22E-2.7$	$11.8-0.25E+12.\xi$	$1.32, 0.51+0.7\xi$	6.2, 0.98, 0.75	15	7	8
Best $r_R=1.22$	$50.0-0.32E+0.4\gamma+24.\xi$	1.22, 0.72	$0.22E-2.7$	$11.8-0.25E+12.\xi$	$1.32, 0.51+0.7\xi$	6.2, 1.06, 0.68	15	7	8
$V_{sym}=0, r_R\propto\xi$	$58.5-0.32+0.4\gamma$	$1.11+0.33\xi, 0.76$	$0.22E-2.7$	$11.8-0.25E+12.\xi$	$1.32, 0.51+0.7\xi$	6.2, 1.01, 0.75	13	8	8
$V_{sym}=0, a_R\propto\xi$	$56.-0.24E+0.4\gamma$	$1.15, 0.66+1.\xi$	$0.22E-2.7$	$11.8-0.25E+12.\xi$	$1.32, 0.51+0.7\xi$	6.2, 1.01, 0.75	14	8	8
$V_C=0$	$57.3-0.32E+28.\xi$	1.17, 0.75	$0.22E-2.7$	$11.8-0.25E+12.\xi$	$1.32, 0.51+0.7\xi$	6.2, 1.01, 0.75	14	8	6
$V_C=0.3$	$54.9-0.32E+0.3\gamma+25.\xi$	1.17, 0.75	$0.22E-2.7$	$11.8-0.25E+12.\xi$	$1.32, 0.51+0.7\xi$	6.2, 1.01, 0.75	12	7	6
$V_{CC}=0.84$ [b]	$55.2-0.32E+0.27\gamma+24\xi$	1.17, 0.75	$0.22E -0.18\gamma -1.4$	$10.2-0.25E +0.21\gamma+12\xi$	$1.32, 0.51+0.7\xi$	6.2, 1.01, 0.75	12	7	6
$r_I'=1.22, a_I'=0.72$ [c]	$54.-0.32E+0.27\gamma+24\xi$	1.17, 0.75	$0.22E-2.7$	$11.8-0.25E+12\xi$	$1.32, 0.51+0.7\xi$	6.2, 1.01, 0.75	13	7	6
$V_{s\,sym}=9$ [d]	$56.-0.32E+0.4\gamma$	1.17, 0.75	$0.22E-2.7$	$11.8-0.25E+12\xi$	$1.32, 0.51+0.7\xi$	6.2, 1.01, 0.75	14	8	7
No so [e]	Search terminated parameters converging very slowly.					0., ···, ···	30	···	12

[a] Using data of Fig. 1 which includes 40 $\sigma(\theta)$, 28 $P(\theta)$, and 8 σ_R data in the 46 data sets. $\gamma=Z/A^{1/3}$, $\xi=(N-Z)/A$, $E=E_{lab}$, and W_V, W_{SF} always ≥ 0.

[b] Variable Coulomb energy term added to all energy-dependent strengths, i.e., incident proton energy E replaced by an effective energy $E-V_{CC}Z/A^{1/3}$ with V_{CC} a search parameter.

[c] Separate geometry used for volume imaginary potential with $W(r) = -W_V f(r, r_I', a_I') + W_{SF}4a_I(d/dr)[f(r,r_I,a_I)]$.

[d] Volume real symmetry term replaced by surface form: $V_{R\,sym}(r) = -V_{S\,sym}\xi 4a_R(d/dr)[f(r,r_R,a_R)]$.

[e] Attempt to fit $\sigma(\theta)$ and σ_R data only without using a spin-orbit potential ($V_{so}=0$).
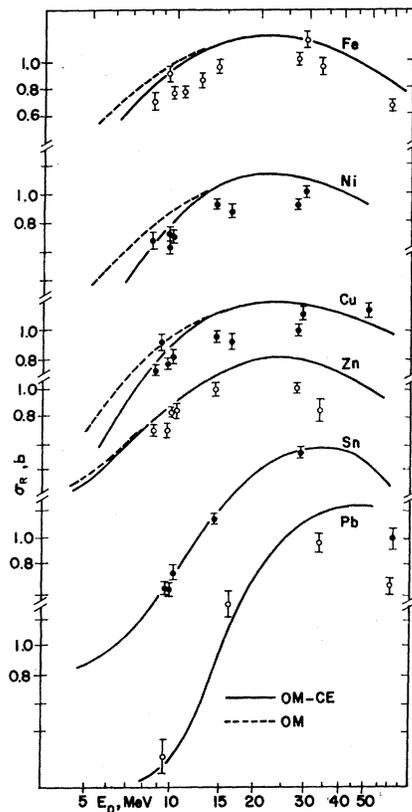
FIG. 4. Comparison of the reaction cross-section predictions with experimental values using the proton best-fit parameters (Refs. 11–16 and 42, 43).

correspond to a minimum in F using the particular parameterization.

The OM predictions given by (8) compared to a range of experimental data are given in Figs. 4–12 (see Refs. 10–44). The average χ^2 value is about ten per point for the 6000 data points shown in these figures. Of these 6000 data points, approximately 2500 were used in the search which yielded Eqs. (8).

Compound elastic scattering corrections have been applied to the low-energy data as given by Eq. (4). The relation of the total correction to the appropriate (p, n) thresholds is shown in Fig. 6. The quantity $\sigma_{CE}{}^{OM}$ is the total correction needed to fit the corresponding $\sigma(\theta)$ data at the energies shown. The scattering appears, then, to approach pure direct elastic scattering for $E \approx Q(p, n) + 4$ MeV. The corrected OM fits to these low-energy data are shown in Fig. 7. The magnitudes of the corrections used are comparable to both measured fluctuations in the cross sections at these energies and calculated values using the Hauser-

Feshbach or statistical model of compound nuclear scattering.[45,46]

The Rutherford Laboratory $\sigma(\theta)$ [16] and $P(\theta)$ [28] data have been included separately at different energies where appropriate. The 40-MeV data analyzed were an average of the Oak Ridge[30] and Minnesota[31] data but separated data are shown with the OM predictions.

The experimental reaction cross sections at different energies, in some cases, represent values obtained by averaging isotopic values.

The over-all agreement with experiment is, in general, quite good $(\chi^2/N \approx 10)$. The most apparent discrepancies are in the OM prediction of the reaction cross sections for the lighter nuclei $(A < 90)$. This may indicate some inadequacy in the basic forms chosen for $W(r)$. Comparable σ_R data at other energies would permit a more thorough investigation of this problem.

Neutron Parameters

The neutron data (Fig. 2) were analyzed using the proton parameters (Table I) as starting values. The
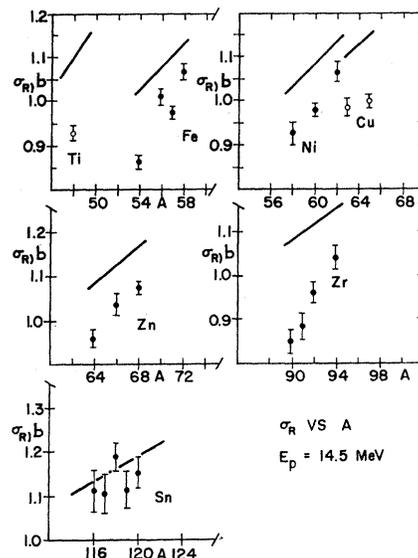
FIG. 5. Comparison of the reaction cross-section predictions for isotopic sequences with experimental values using the proton best-fit parameters (Ref. 15).

---

[42] T. J. Gooding, Nucl. Phys. **12**, 241 (1959).
[43] Verena Meyer, R. M. Eisberg, and R. F. Carlson, Phys. Rev. **117**, 1334 (1959).
[44] N. M. Hintz, Phys. Rev. **106**, 1201 (1957).

[45] W. Hauser and H. Feshbach, Phys. Rev. **87**, 366 (1952); T. Ericson, Ann. Phys. (N.Y.) **23**, 390 (1963); J. Ernst, P. Von Brentano, and T. Mayer-Kuckuk, Phys. Letters **19**, 41 (1965).
[46] The improvement effected in Fig. 7 and the agreement with estimates obtained using Ref. 45 constitute the best justification for the assumption made here concerning the isotropic nature of the compound elastic contribution. Appreciable anisotropies are expected when high spin values are involved [see L. Wolfenstein, Phys. Rev. **82**, 690 (1951)], but these represent departures at forward (<40°) and backward (>140°) angles. For protons, the forward angle region is dominated by Coulomb scattering and little of the data used here is at backward angles, so that, in the present proton analysis, the isotropic compound elastic assumption is probably satisfactory.

results, however, were insensitive to small changes in the energy and $(N-Z)/A$ terms. As a conseqneuce, the energy dependence of the central strengths was set equal to that of the corresponding proton terms. Also, the $(N-Z)/A$ dependence of the strengths could be set equal to the negative of the proton values. This is as expected for an isospin-dependent potential of the form $(V+iW)\mathbf{t}\cdot\mathbf{\tau}$, where $\mathbf{t}$ is the incident isospin and $\mathbf{\tau}$ the target nucleus isospin.[47,48] The imaginary diffuseness showed no systematic features and was subsequently assumed to be constant. The real geometry and spin-orbit strength and geometry did not change significantly from the proton parameters and these too could be set equal to the proton values. The most
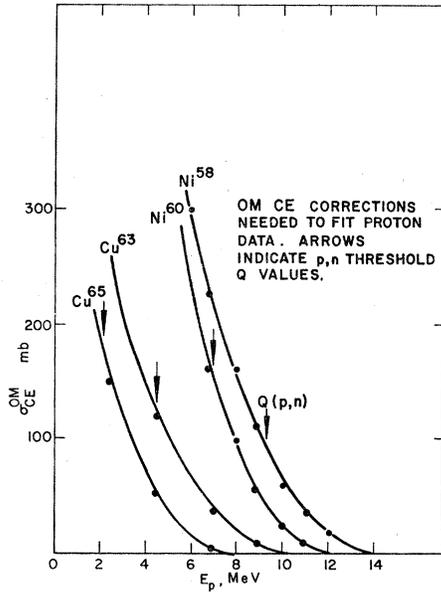
FIG. 6. The total isotropic compound elastic corrections found for protons as a function of energy.

significant changes were in the strength and geometry of the absorptive potential which indicated a smaller radius and an increased volume strength for neutrons (see Fig. 13). A slight difference in the proton and neutron real central strengths V_R was also found. This can be removed by using a Coulomb correction term of $0.27Z/A^{1/3}$ instead of the usual $0.4Z/A^{1/3}$ in the proton potential (see Tables I and II). The neutron data were also found to be fitted slightly better using a surface-peaked real symmetry term. The significance of this will be discussed in Sec. IV.

The best fit to the neutron data, using the energy and isospin dependence from the best fit to the proton data,

[47] A. M. Lane, Nucl. Phys. 35, 676 (1962).
[48] G. R. Satchler, Nucl. Phys. A91, 75 (1967).

TABLE II. A listing of the parameters found in the analysis of the neutron data of Fig. 2 using different potential forms. Only those forms giving reasonable fits to the data have been included.

Comments[a]	V_R (MeV)	r_R, a_R (F)	W_V (MeV)	W_{SF} (MeV)	r_I, a_I (F)	V_{so}, r_{so}, a_{so} (MeV, F, F)	$\sigma(\theta)$	$\langle x^2/N \rangle$	$P(\theta)$	σ_R
Best fit	$56.3-0.32E-24.\xi$	$1.17, 0.75$	$0.22E-1.6$	$13.-0.25E-12.\xi$	$1.26, 0.58$	$6.2, 1.01, 0.75$	2.2	2	2	4
Use$+V_{sym}$	$55.-0.31E+24.\xi$	$1.15, 0.74$	$0.22E-1.6$	$13.-0.25E-12.\xi$	$1.26, 0.58$	$6.2, 1.01, 0.75$	12	7	7	8
Use$+W_{sym}$	$56.3-0.32E-24.\xi$	$1.17, 0.75$	$0.22E-1.6$	$13.-0.25E+12.\xi$	$1.27, 0.60$	$6.2, 1.01, 0.75$	3	2	2	6
$a_I \propto -\xi$	$56.3-0.32E-24.\xi$	$1.17, 0.75$	$0.22E-1.6$	$13.8-0.25E-11.\xi$	$1.27, 0.6-0.7\xi$	$6.2, 1.01, 0.75$	2.4	2	2	5
$a_I \propto +\xi$	$56.3-0.32E-24.\xi$	$1.17, 0.75$	$0.22E-1.6$	$13.-0.25E-12.\xi$	$1.27, 0.5+0.7\xi$	$6.2, 1.01, 0.75$	2.5	2	2	5
$a_I \propto E$	$56.3-0.32E-24.\xi$	$1.17, 0.75$	$0.22E-1.6$	$13.-0.25E-12.\xi$	$1.3, 0.5+0.008E$	$6.2, 1.01, 0.75$	2.3	2	2	4
$W_V \propto \xi$	$56.3-0.32E-24.\xi$	$1.17, 0.75$	$0.22E-1.6-1.\xi$	$13.-0.25E-12.\xi$	$1.26, 0.54$	$6.2, 1.01, 0.75$	2.4	2	2	3
$r_{so}=r_R=1.17$	$56.3-0.32E-24.\xi$	$1.17, 0.75$	$0.22E-1.6$	$12.-0.25E-12.\xi$	$1.26, 0.58$	$6.4, 1.17, 0.58$	3	4	4	4
Common[b]	$55.2-0.32E-24.\xi$	$1.17, 0.75$	$0.22E-1.4$	$12.-0.25E-12.\xi$	$1.26, 0.58$	$6.2, 1.01, 0.75$	2.7	4	4	3
$V_{Ssym}=9$[c]	$53.2-0.32E$	$1.17, 0.75$	$0.22E-1.6$	$13.-0.25E-12.\xi$	$1.26, 0.58$	$6.2, 1.01, 0.75$	2.0	2	2	4

a $\gamma = Z/A^{1/3}$, $\xi = (N-Z)/A$, W_V, $W_{sf} \geqslant 0$, $E = E_{lab}$. Data used is shown in Fig. 2 and includes $30\sigma(\theta)$, $4 P(\theta)$, $28 \sigma_T$ data sets.
b Potential similar to proton potential with Coulomb correction in all the strengths.
c Volume real symmetry term replaced by surface form: $V_{R\,sym}(r) = +V_{S\,sym}\,\xi\,4a_R(d/dr)$ $|f(r, r_R, a_R)|$.
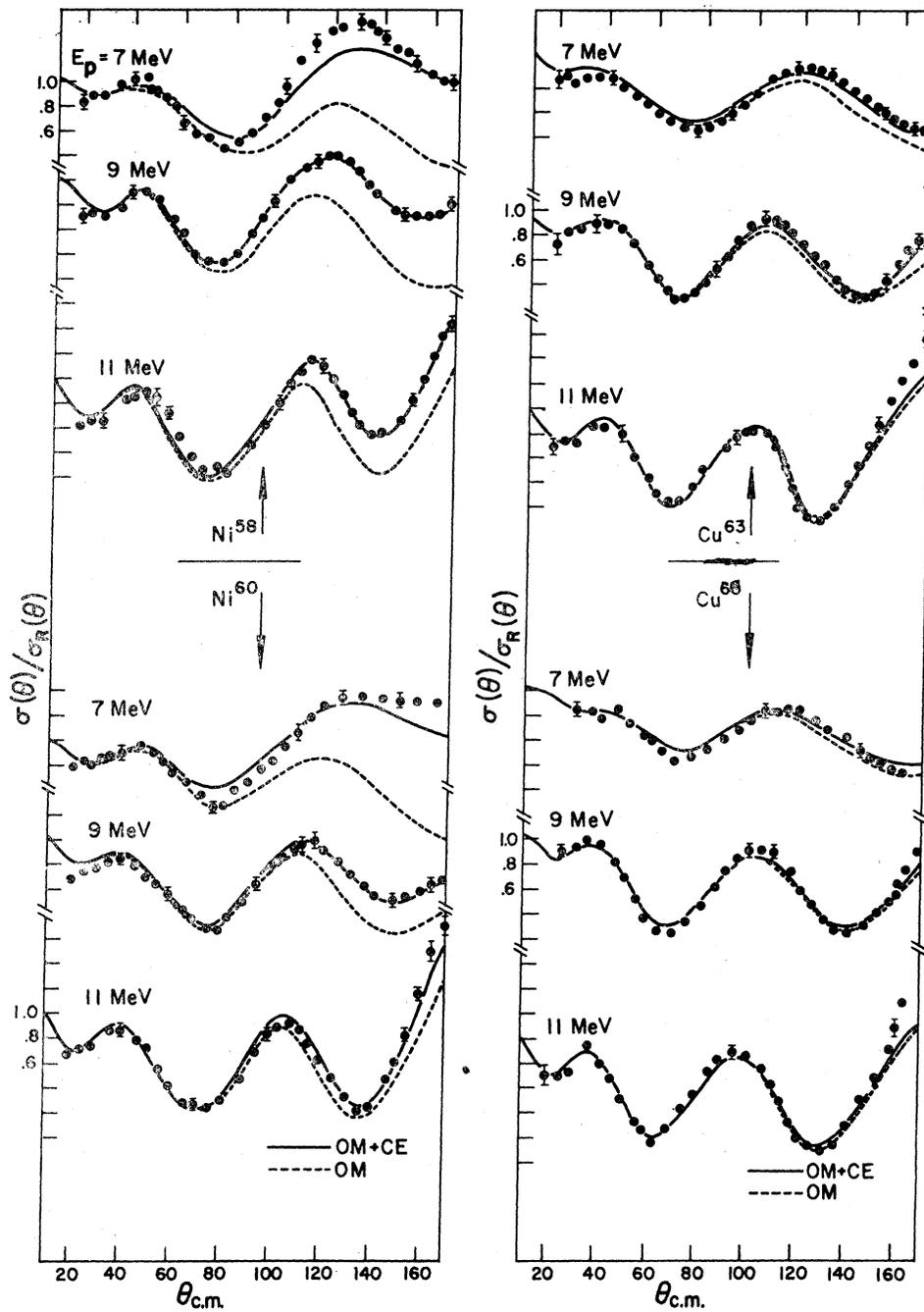
FIG. 7. Comparison of experimental cross-section data with the best-fit predictions for protons, $E_p = 7$–11 MeV (Ref. 10).

was obtained using the parameters

$$V_R = 56.3 - 0.32E - 24.0(N-Z)/A,$$

$$r_R = 1.17, \qquad a_R = 0.75,$$

$W_v = 0.22E - 1.56$ or zero whichever is greater,

$$W_{\mathrm{SF}} = 13.0 - 0.25E - 12.0(N-Z)/A$$

or zero, whichever is greater,   (9)

$$r_I = r_I' = 1.26, \qquad a_I = a_I' = 0.58,$$

$$V_{\mathrm{so}} = 6.2,$$

$$r_{\mathrm{so}} = 1.01, \qquad a_{\mathrm{so}} = 0.75,$$

where E is the incident neutron lab energy in MeV.

The listing of the neutron parameters examined is given in Table II. Average neutron and mass numbers N, A have been used for the natural targets.
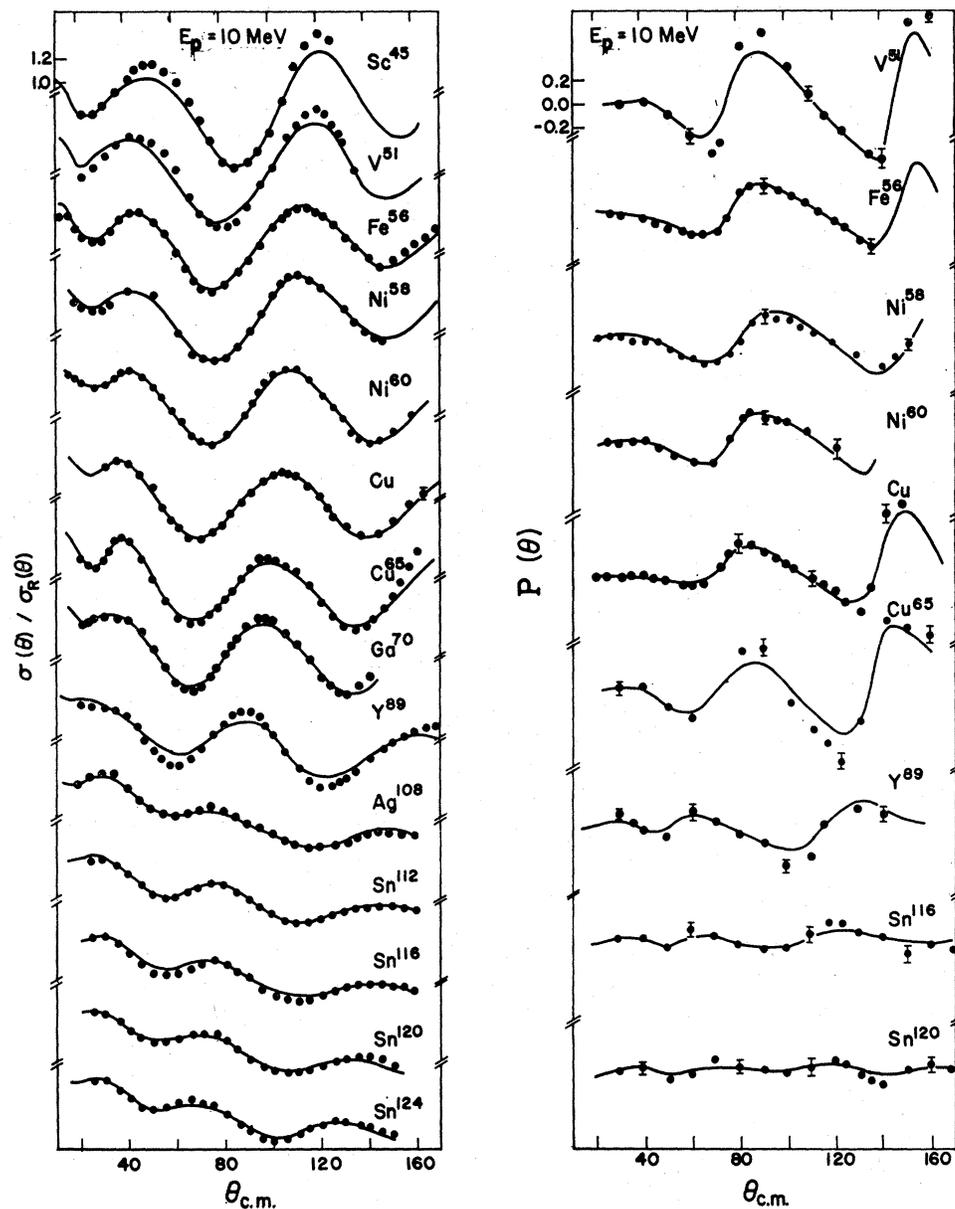
FIG. 8. Comparison of experimental cross-section data with the best-fit predictions for protons, $E_p = 10$ MeV. $\sigma(\theta)/\sigma_R(\theta)$ (Refs. 17–19, 44) and $P(\theta)$ (Refs. 20, 21).

The most significant difference between the proton parameters of Eqs. (8) and the neutron parameters of Eqs. (9) is in the strength and geometry of $W(r)$. This is illustrated in Fig. 13, which shows $W(r)$ for both protons and neutrons on Sn^{120} at various energies. The origin of this difference is discussed later in this paper.

The OM fits to a large sample of neutron data using the parameters of Eq. (9) are given in Figs. 14–18

(see Refs. 33–39, 49). Again, at low energies ($E < 10$ MeV) corrections for compound elastic scattering are necessary for both $\sigma(\theta)$ and σ_R data. The corrections given by Eqs. (4) also improve the fit to the low-energy polarization data slightly, reducing χ^2/N values by 10–20% (see Fig. 17). In all instances, the compound

[49] G. V. Gorlov, N. S. Lebedeva, and U. M. Morozov, Dokl. Akad. Nauk SSSR 158, 574 (1964) [English transl.: Soviet Phys.—Doklady 9, 806 (1965)].
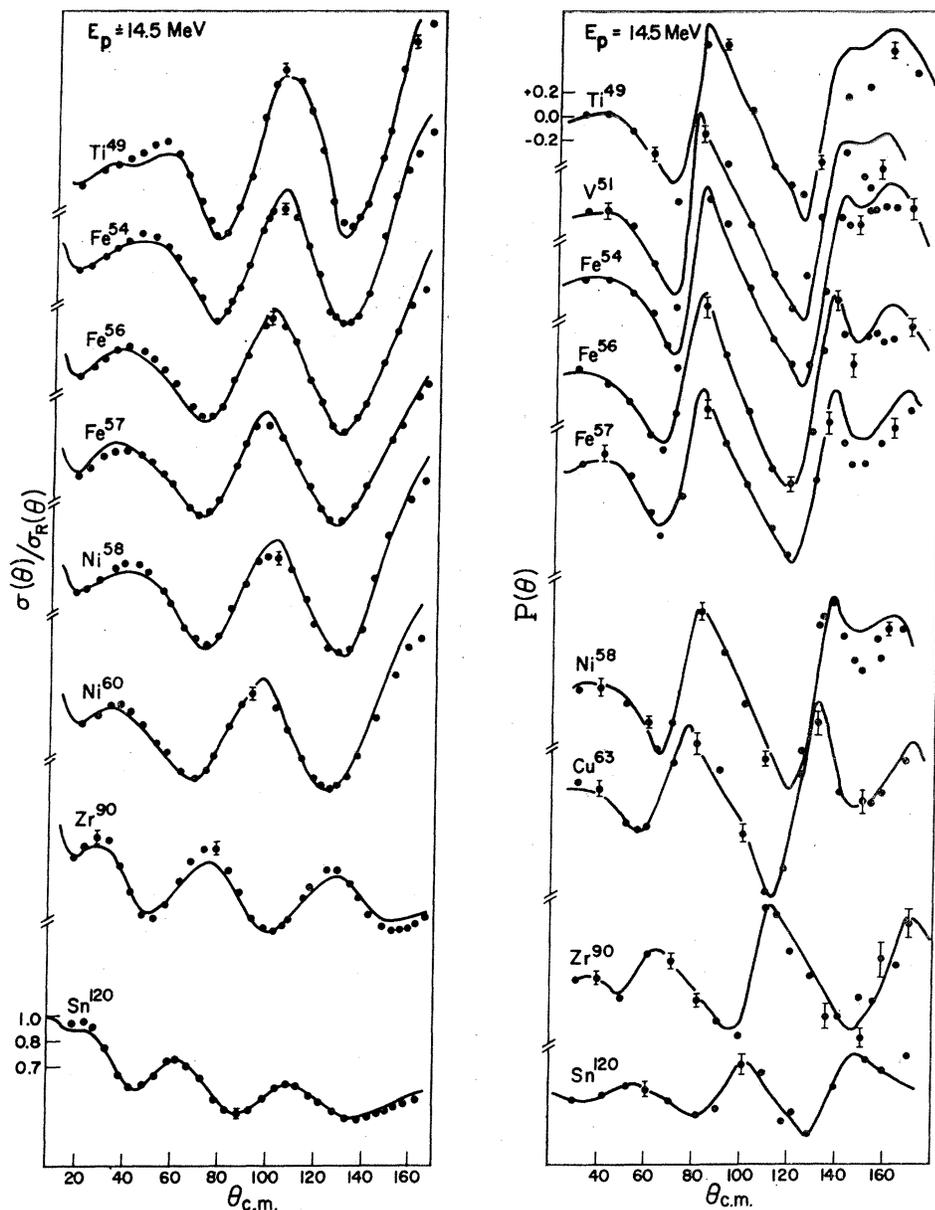
FIG 9. Comparison of experimental cross-section and polarization data with the best-fit predictions for protons, $E_p = 14.5$ MeV. $\sigma(\theta)/\sigma_R(\theta)$ (Ref. 22) and $P(\theta)$ (Ref. 21).

elastic corrections required were consistent among data at different energies, with typical values expected.[45,46,50]

[50] The compound elastic corrections needed for the neutron data were in some cases quite sizeable. This raises doubts as to the validity of the isotropic assumption for these corrections. Anisotropies have been observed [see L. Cranberg *et al.*, Phys. Rev. Letters, 11, 341 (1963)], which were significant at forward (<40°) and backward (>140°) angles. Although the neutron data analyzed here are dominated by results for the angular region 40°–140°, it does include some forward and backward angle data. It is unlikely that nonisotropic compound elastic effects will significantly affect the parameters found here, but their possible presence does further emphasize the need for caution in the use of the results of the present neutron analysis.

Analogous to the OM fit to the proton data, the fit to the neutron data is poorest for total cross sections for the lighter nuclei $(A<90)$, and again indicates a basic inadequacy in the present optical potential.

Data $A<40$

An attempt was made to fit elastic data for nuclei $A<40$ using the form of parameterization found for the heavier nuclei. While a reasonable OM fit could be obtained for forward angle data $(\theta<90°)$, the large-angle points could be fitted only by allowing adjust-
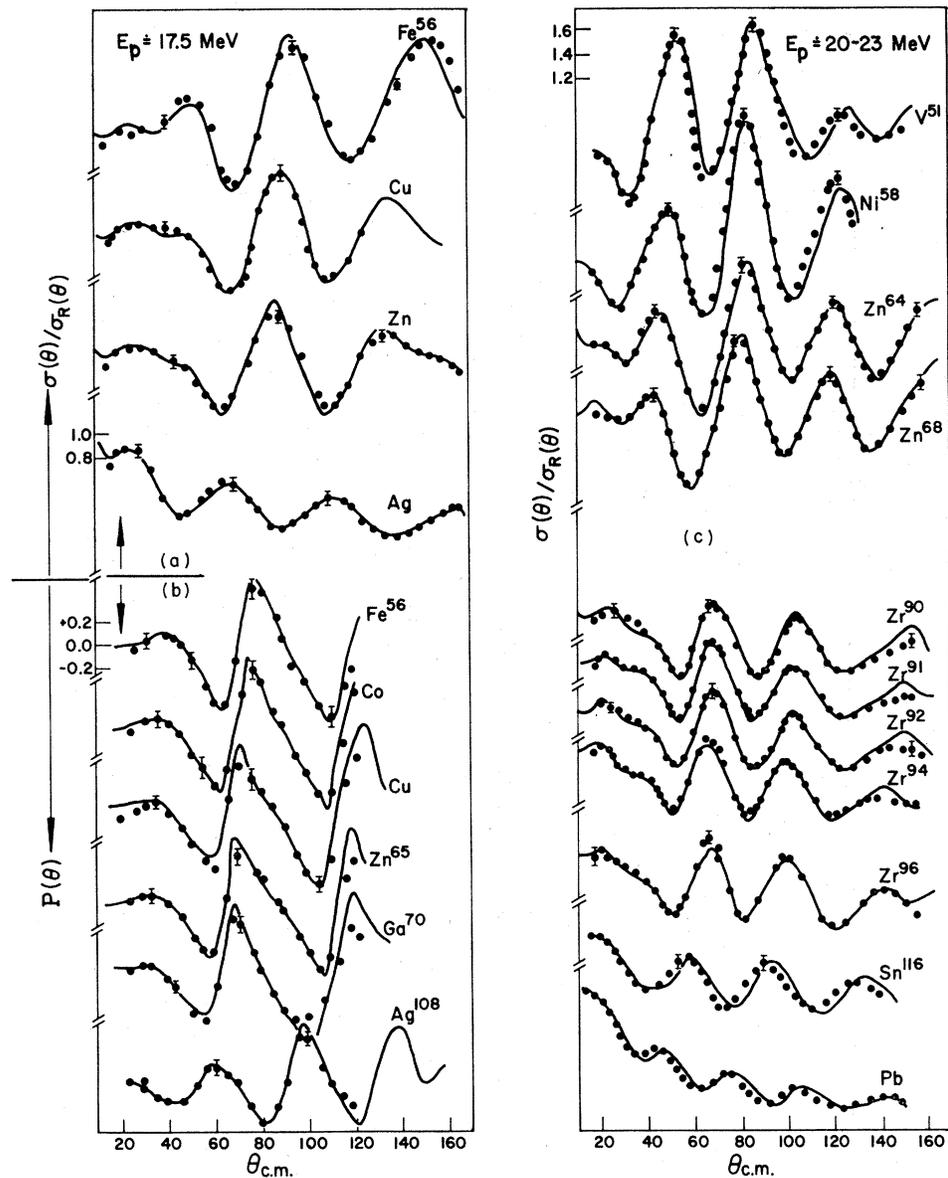
FIG 10. Comparison of experimental cross-section and polarization data with the best-fit predictions for protons, $E_p = 17$–23 MeV. (a) Ref. 23, (b) Ref. 24, and (c) Refs. 25, 26.

ments to the OM parameters, particularly r_I, which required a substantial increase. This increase in r_I suggests that $R_I \neq r_I A^{1/3}$ in light nuclei, as expected for a long-range interaction such as $W(r)$. Also unlike the heavier elements, relatively few nonelastic channels determine the absorbtion and the simple form of $W(r)$ used is no longer appropriate.

V. SUMMARY OF RESULTS

The main features revealed in the present standard OM analysis of data $A > 40$, $E < 50$ MeV are as follows:

(a) The real and imaginary strengths are linearly dependent on incident energy with

$$V_R \propto -(0.32 \pm 0.02)E,$$

$$W_V \propto +(0.22 \pm 0.04)E,$$

$$W_{SF} \propto -(0.25 \pm 0.02)E.$$

(The errors quoted correspond to a change in the criterion function F of approximately 20% as determined from the parameter iterations.)

(b) The real central potential can be specified by several different combinations of parameters within the
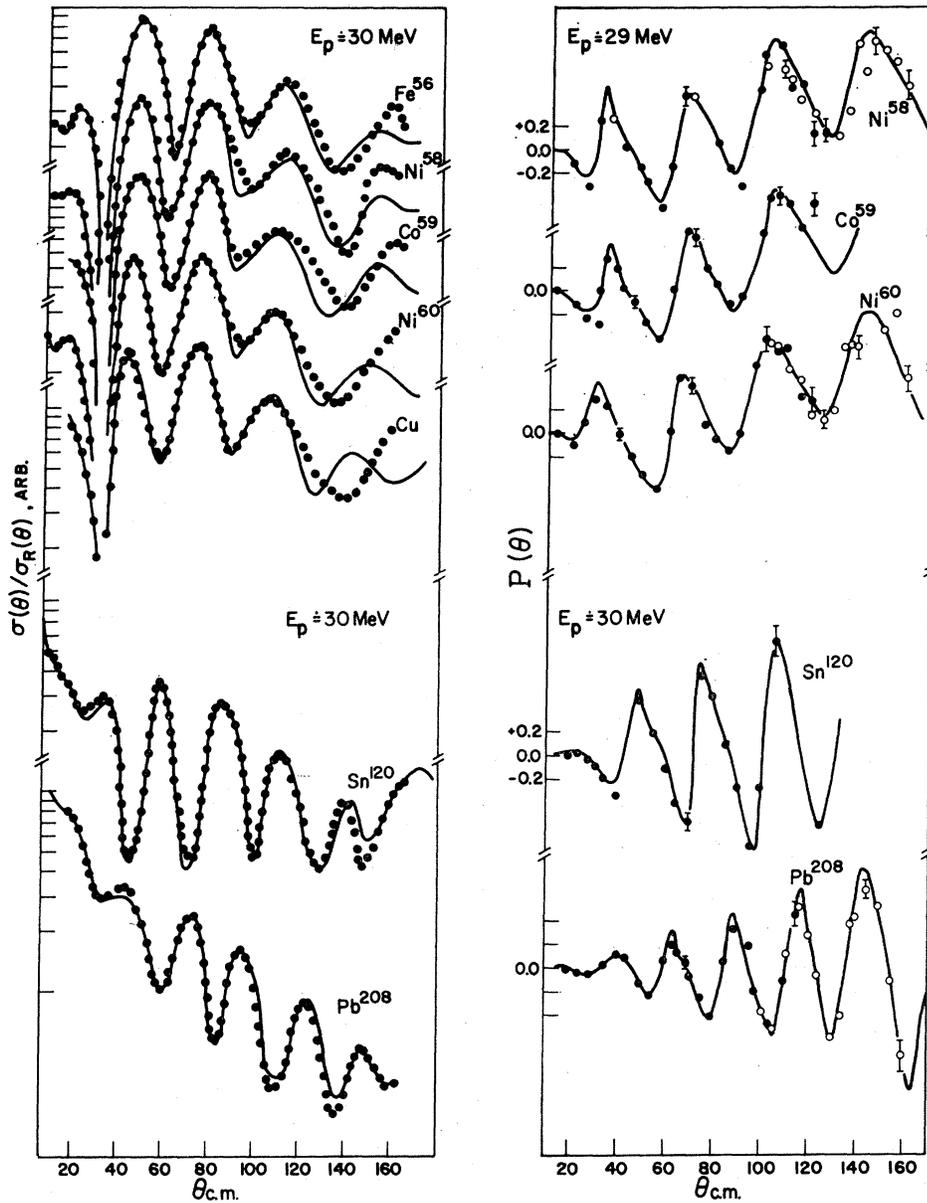
FIG. 11. Comparison of experimental cross-section and polarization data with the best-fit predictions for protons. $E_p = 30$ MeV, ● (Ref. 27); $E_p = 29$ MeV, ● (Ref. 28), ○ (Ref. 29).

range

$$1.10 < r_R < 1.25,$$

$$0.70 < a_R < 0.78,$$

$$59 > V_R > 52.$$

(c) A constant spin-orbit strength

$$V_{so} = 6.2 \pm 1.0.$$

(d) A complex isospin potential with real volume term,

$$V_{sym} = 24 \pm 3 \text{ (Coulomb correction of } 0.4Z/A^{1/3})$$

or

$$V_{sym} = 30 \pm 3 \text{ (no Coulomb correction)},$$

and a surface-peaked imaginary term,

$$W_{sym} = 12 \pm 3.$$

The neutron data are fitted slightly better using a surface-peaked real isospin term with $V_{S\,sym} = 9 \pm 2$.

VI. DISCUSSION

The best-fit OM potentials for protons and neutrons were obtained from a simultaneous fitting of a com-
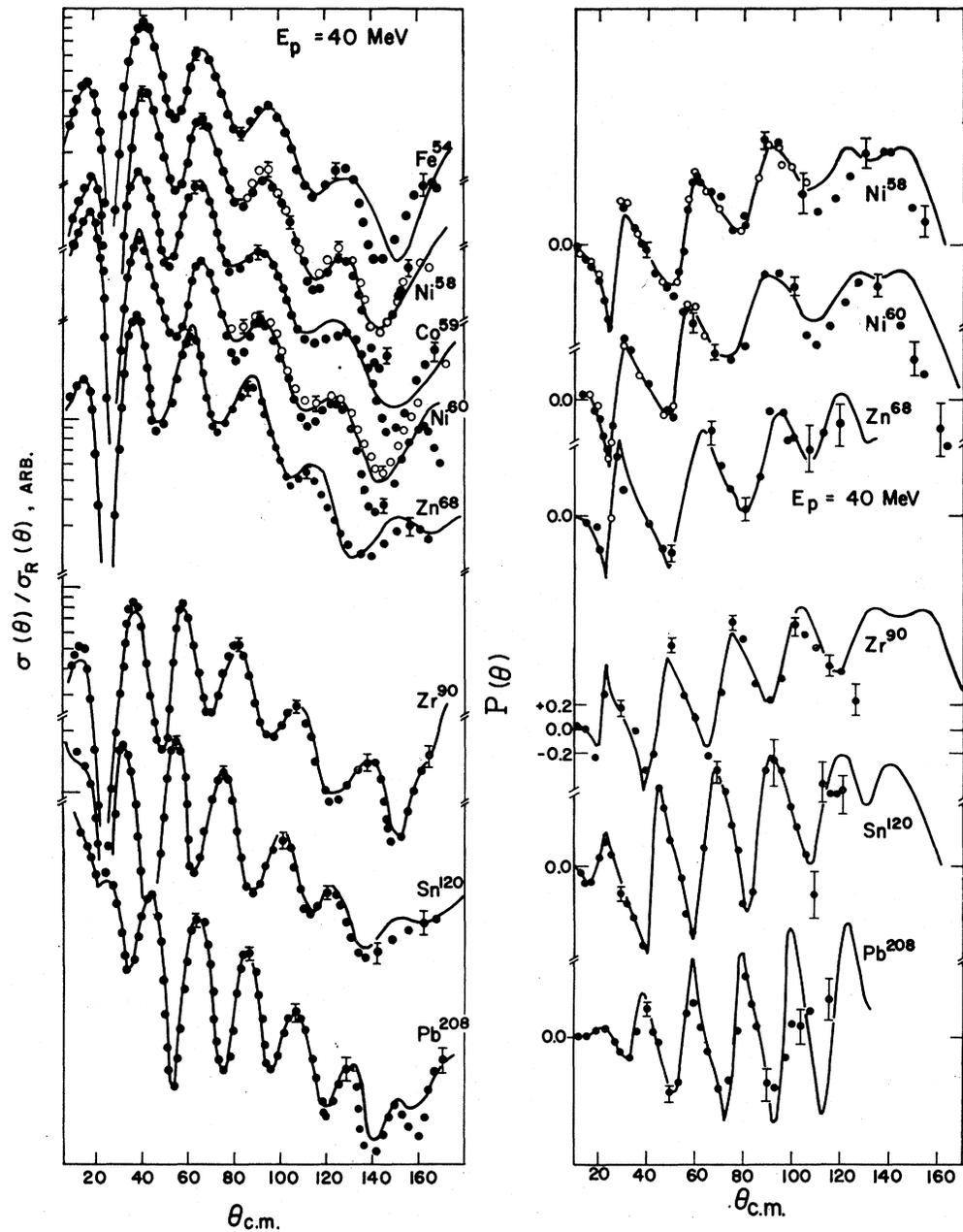
FIG. 12. Comparison of experimental cross-section and polarization data with the best-fit predictions for protons, $E_p = 40$ MeV. $\sigma(\theta)/\sigma_R(\theta)$, ● (Ref. 30) and ○ (Ref. 31); $P(\theta)$, ● (Ref. 30) and ○ (Ref. 32).

prehensive and representative set of (a) all available proton data [Eq. (8)] and (b) all available neutron data [Eq. (9)] in the energy range below 50 MeV. These potentials, therefore, represent the best over-all parameterization of the scattering using the standard formulation of the OM. Implicit in such a formulation are certain assumptions in the functional forms used. Perhaps the most questionable of these assumptions

is that of an $A^{1/3}$ dependence for all of the radius parameters (real central, imaginary central, and spin-orbit). The functional form used for the imaginary central potential also gives cause for concern, since severe ambiguity problems are often experienced with this term and an alternate shape might be more satisfactory. Such doubts as to the validity of the initial assumptions limit the extent to which physical significance
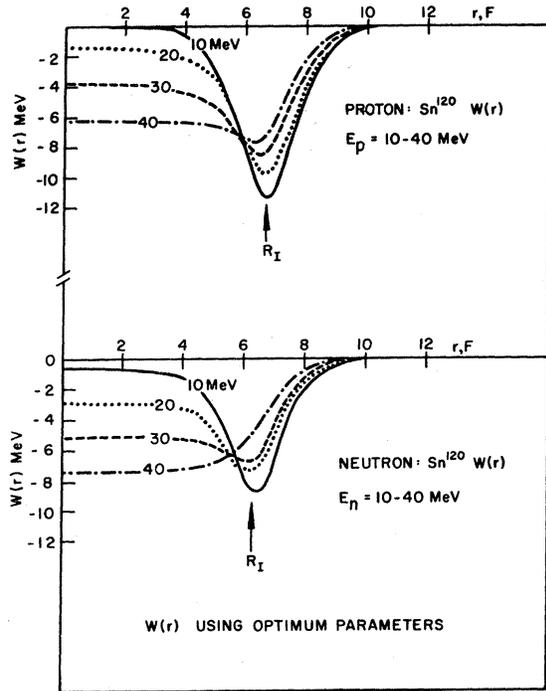
Fig. 13. Plots of the best-fit neutron and proton imaginary potentials found for Sn^{120}.

can be attached to the results. These reservations are strongly enhanced by the wide variety of parameterizations which have been found to yield fits to the data and which are almost as good as the optimum fit (see Tables I and II) and it is, in fact, impossible, with the present formulation, to determine a unique set of strength and geometry parameters which is significantly superior to several other sets. The parameters determined must be considered primarily as phenomenological representations of complex phase shifts. The parameter ambiguities are inherent in the formulation used and are essentially independent of the amount of data included in the analysis. Nonetheless, the results obtained with various parameterizations do have common features which, almost certainly, can be related to the physical processes involved. These are discussed later in this section.

From a utilitarian point of view, as long as the limitations are recognized and the alternate potentials quoted are treated as convenient representations of the data, they should prove useful for predicting elastic cross sections and polarizations below 50 MeV and for calculations involving the distortion of proton and neutron reaction channels. The use of Eqs. (8) and (9) for energies greater than 50 MeV and mass numbers less than 40 may not be reliable. At higher energies, the potential strengths may no longer have a linear energy dependence and for lighter nuclei, considerable changes in the imaginary geometry may be necessary (see Sec. IV).

Recently, a reformulation of the OM has been presented by Greenlees, Pyle, and Tang (GPT)[51] which avoids some of the difficulties of the normal formulation and attempts to relate the real parts of the OM potential to the nuclear matter distribution and specific components of the nucleon-nucleon force. GPT showed that the well-defined quantities involved in the analysis of proton elastic scattering data are the volume integrals (J_R) and the mean-square radii (msr) $(\langle r^2 \rangle_R)$ of the real central potential. In their formulation of the problem, $\langle r^2 \rangle_R$ is related to the msr of the nuclear matter distribution $(\langle r^2 \rangle_m)$ via the relation

$$\langle r^2 \rangle_R = \langle r^2 \rangle_m + \langle r^2 \rangle_d, \qquad (10)$$

where $\langle r^2 \rangle_d$ is the msr of the spin-isospin–independent part of the nucleon-nucleon potential. Also, to a good approximation,

$$\langle r^2 \rangle_m = \langle r^2 \rangle_{so}, \qquad (11)$$

where $\langle r^2 \rangle_{so}$ is the msr of the spin-orbit form factor. The nuclear matter msr found by GPT were independent of the incident proton energy in the range examined (14–40 MeV) and the volume integrals suggested a slow decrease with energy. The standard OM formulation used in the present paper yields satisfactory fits to all the available data below 50 MeV and it is of interest to compare the results with the conclusions of GPT who analyzed part of these data in considerable detail using a different approach.

The proton parameters of Eq. (8) enable $\langle r^2 \rangle_R$ and J_R to be calculated for any A and E, and taking $\langle r^2 \rangle_d = 2.25$ F^2 as determined by GPT,[52] yields values for $\langle r^2 \rangle_m^{1/2}$, the rms radius of the nuclear matter distribution. The values of $\langle r^2 \rangle_m^{1/2}$ and J_R/A for $A = 60$, 120, and 208 at various energies are given in Table III, together with the same quantities as determined by GPT. The agreement between the two sets of data is excellent. The values quoted in Table III, for the present work, were obtained using the best-fit parameters.

GPT analyzed data for individual elements and energies independently and showed that, whereas the radius and diffuseness parameters could have a wide range of values, the rms radii were well defined. Using Eq. (10) with $\langle r^2 \rangle_d = 2.25$ F^2 as in GPT, the present analysis of more data in a different manner yields the same values for $\langle r^2 \rangle_m^{1/2}$ and J_R/A and strongly supports the conclusion of GPT that these are the quantities which must be specified in order to fit proton elastic scattering data. The restriction imposed here of an $A^{1/3}$ variation for the radius parameters with constant

[51] G. W. Greenlees, G. J. Pyle, and Y. C. Tang, Phys. Rev. **171**, 1115 (1968).

[52] It has recently been suggested [see Slanina and McManus, Nucl. Phys. **A116**, 271 (1968)] that a somewhat higher value for $\langle r^2 \rangle_d$ might be more appropriate. Such a value would reduce the $\langle r^2 \rangle_m$ values, via Eq. (10), but does not affect the general conclusions drawn here.
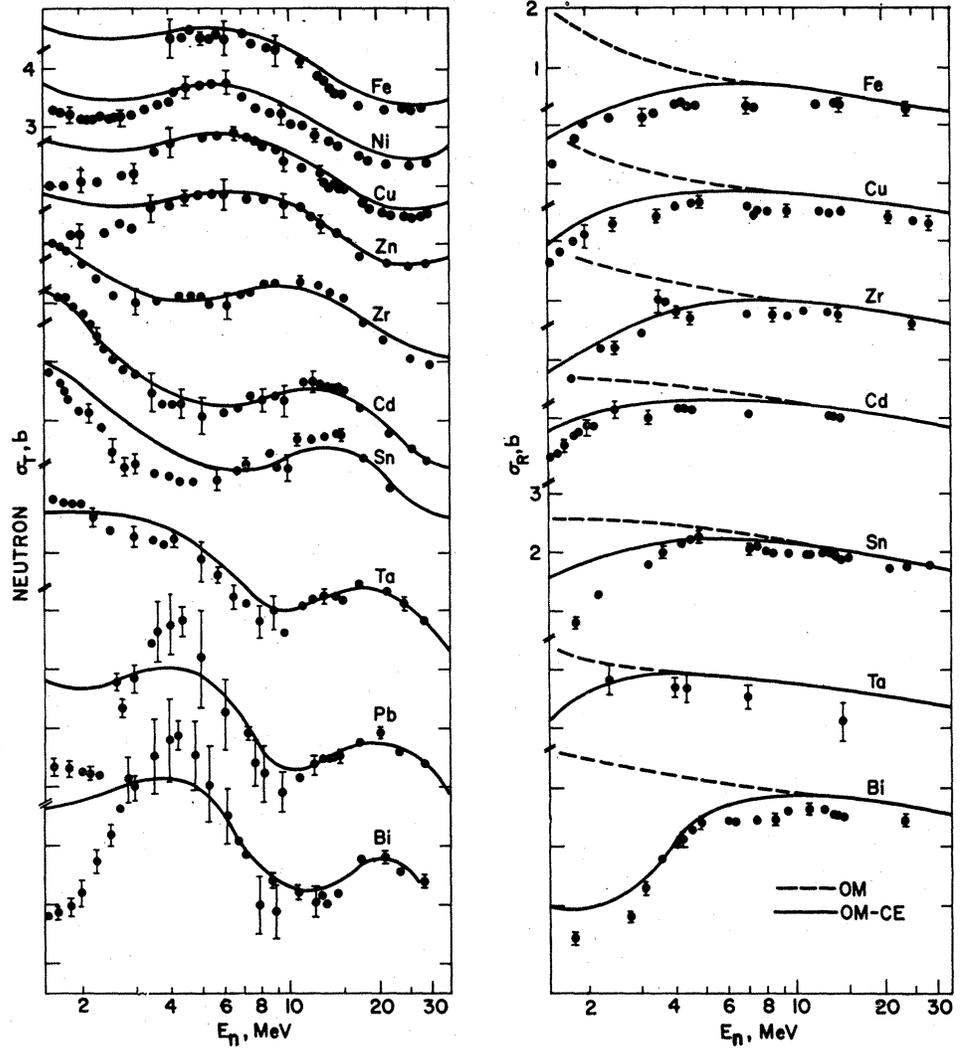
FIG. 14. Comparison of the total and reaction cross-section predictions with experimental values using the neutron best-fit parameters (Ref. 33).

a_R predetermines the variation of $\langle r^2 \rangle_m$ with A for a given r_R and a_R. The optimum values found for these parameters are clearly those which give the best values for J_R/A and $\langle r^2 \rangle_m^{1/2}$ over the range of A. The minor discrepancy in $\langle r^2 \rangle_m^{1/2}$ for Ni^{60} (4.26 compared to 4.15±0.05F) is very probably due to this constraint of an $A^{1/3}$ variation of R_R. An additional minor source of discrepancy could be the different functional form of $V_R(r)$ used in the two treatments; there is, however, no evidence that this is significant. The excellent agreement in $\langle r^2 \rangle_m^{1/2}$ obtained with the two approaches lends strong support to the physical basis of the GPT formulation and suggests that the present real central geometry together with Eq. (10) gives the over-all variation of nuclear matter distribution.[52] When the J_R and $\langle r^2 \rangle_R$ values are calculated using the alternate parameterizations of Table I, minor variations are found from the values quoted in Table III. These variations are found to be correlated with the geo-metrical restrictions imposed by the particular parameterization.

The nuclear matter msr quoted here are significantly greater than the corresponding proton quantities as determined by electron scattering and μ-mesonic x-ray studies and indicate a greater extension of nuclear-neutron distributions as compared to protons. This immediately suggests that the isospin term of the potential does not have the volume form used here. However, this term makes a relatively small contribution to the potential so that the use of a volume form probably does not represent a serious error. In the GPT formulation,[51] a relation between volume integrals is found which is independent of the form factor of the isospin term in the optical potential, viz.,

$$J_R = J_d A\left(1 \pm \zeta \frac{N-Z}{A}\right), \quad \begin{array}{l} +\text{protons,} \\ \\ -\text{neutrons,} \end{array} \quad (12)$$

TABLE III. Comparison of volume integral and rms radius values obtained here with those of Ref. 51.

Isotope	E proton (MeV)	J_R/A Present work (MeV F³)	GPT (MeV F³)	$\langle r^2 \rangle_m^{1/2}$ Present work (F)	GPT (F)
Ni⁶⁰	14.5	455	445±11	4.26	4.14±0.15
	30.3	415	413±10	4.26	4.16±0.05
Sn¹²⁰	14.5	448	454±10	5.05	5.05±0.16
	30.3	411	406±8	5.05	5.02±0.14
Pb²⁰⁸	30.3	412	411±12	5.86	5.84±0.30
	40.0	388	371±14	5.86	5.84±0.35

where J_d is the volume integral of the spin-isospin–independent part of the nucleon-nucleon potential, and ζ is the ratio of the coefficients of the isospin-dependent part of the nucleon-nucleon potential to the spin-isospin–independent part. This relationship assumes the same form factors for the spin-isospin–independent and the isospin-dependent parts of the nucleon-nucleon potential. The energy dependence found in J_R in Ref. 51 was attributed to an energy dependence of J_d.

Proton and neutron potentials are given in Tables I and II which, for a given energy, yield a volume integral relationship similar to Eq. (12). These potentials gave fits to the data as good as the "best" fit for protons and almost as good for neutrons and had real central parts as follows:

$$V_{Rp} = 55.2 - 0.32E + 24(N-Z)/A + 0.27Z/A^{1/3} \text{ MeV,}$$

$$V_{Rn} = 55.2 - 0.32E - 24(N-Z)/A \text{ MeV,} \qquad (13)$$

with

$$r_R = 1.17 \text{ F} \quad \text{and} \quad a_R = 0.75 \text{ F.}$$

A comparison of the coefficients of the $(N-Z)/A$ terms in Eqs. (12) and (13) yields a value for ζ, at 30 MeV, of 0.53. This is in reasonable agreement with the value of 0.48 obtained from the analysis of nucleon-nucleon scattering data.[53–55] The coefficient of the Coulomb term in the proton potential of Eq. (13) (0.27) is necessary to make the magnitudes of the terms in the proton and neutron potentials compatible (see Tables I and II). If this is not required a range from 0 to 0.6 is allowed (Table I). This choice of 0.27 is less than that normally used (0.4). The latter value is obtained by combining the average Coulomb energy inside the nucleus with the energy dependence of the potential. Since the scattering is dominated by the surface region

of the nucleus, where the Coulomb energy is less than at the center, a reduced coefficient is not unexpected.

The imaginary central potentials found for protons and neutrons show qualitative differences. These potentials are plotted at four energies for Sn¹²⁰ in Fig. 13. It is seen in this figure that the proton potential is displaced to larger radii by about 0.3 F and has a greater magnitude in the surface region compared to the neutron potential. These features are readily understood as reflecting the neutron excess in the nuclear surface implied by the rms matter radius being greater than the rms proton radius. An incoming proton inter-
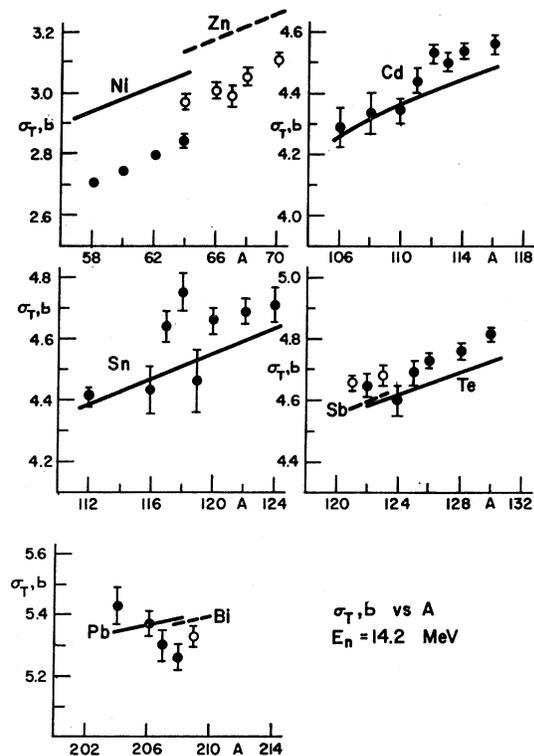
FIG. 15. Comparison of the total cross-section predictions for isotopic sequences with experimental values using the neutron best-fit parameters (Ref. 34).

[53] Y. C. Tang, E. Schmid, and K. Wildermuth, Phys. Rev. 131, 2631 (1963).

[54] S. Oaki and S. C. Park, Phys. Rev. 145, 787 (1966).

[55] D. R. Thompson and Y. C. Tang, Phys. Rev. 159, 806 (1967).
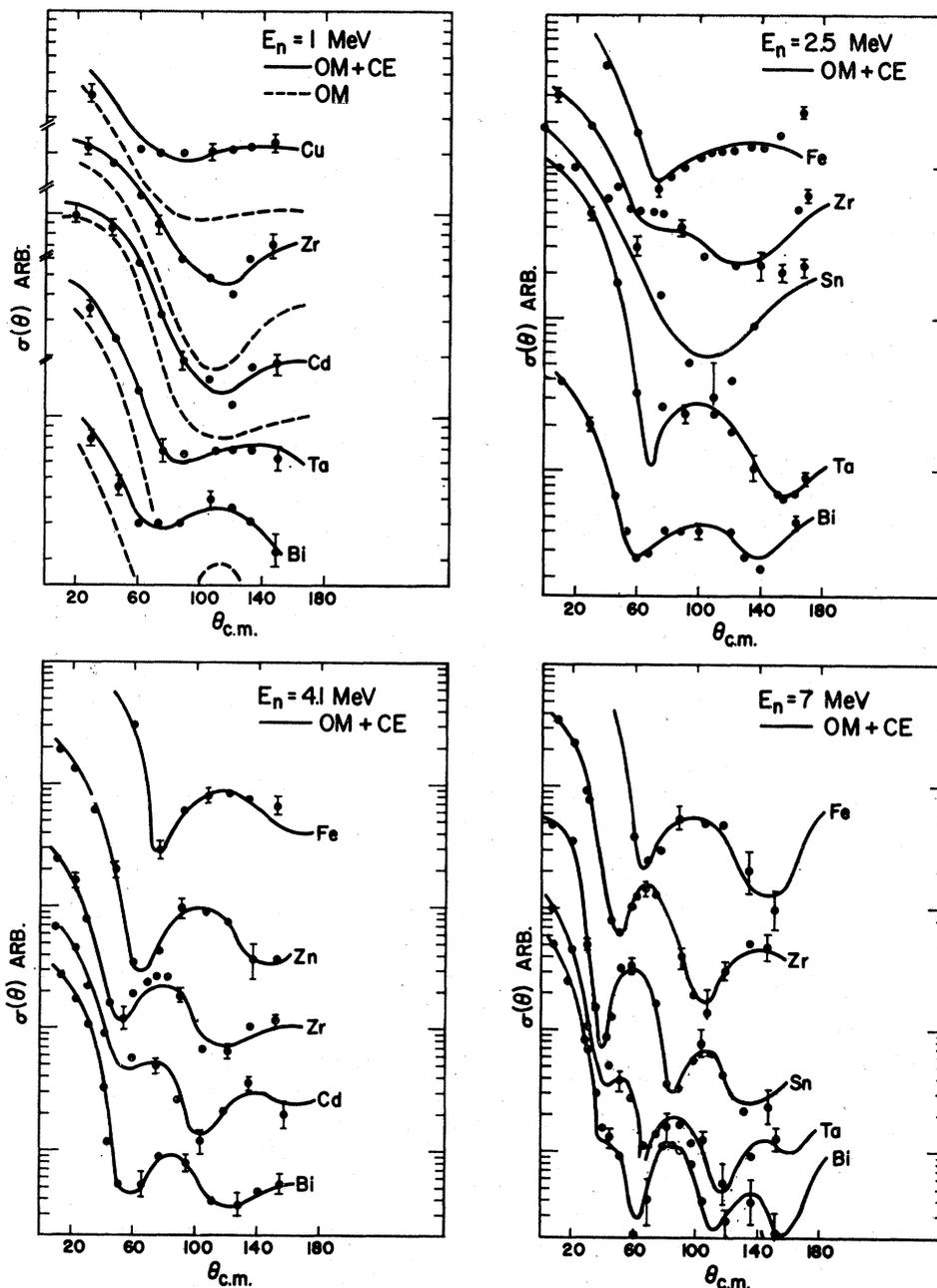
FIG. 16. Comparison of experimental cross-section data with the best-fit predictions for neutrons, $E_n=$ 1–7 MeV (Ref. 35).

acts more strongly with the nuclear neutrons than an incoming neutron because of the absence of triplet scattering in the latter case. The reverse is true for the interactions with nuclear protons. This leads, qualitatively at least, to the features shown in Fig. 13. The radial displacement of the two potentials is comparable to the difference in the nuclear neutron and proton rms radii (approximately 0.6 F for Sn^{120}) implied by the matter radii discussed earlier.[51] The imaginary potentials found, therefore, provide confirmation of the earlier conclusions concerning matter radii.

The imaginary central potentials show an energy and

isospin dependence which, whilst not unexpected, cannot be considered to be quantitatively well speficied in view of the many alternative forms of the potentials found and the limited amount of neutron data available. It will be difficult to define these potentials uniquely in a manner similar to that attempted for the real central potential because of the inherent complexity of the origin of this term.

A further indication of the extent of neutron excess is obtained from the real part of the isospin potential. The symmetry term determined in the present analysis represents a suitable average for a range of nuclei and
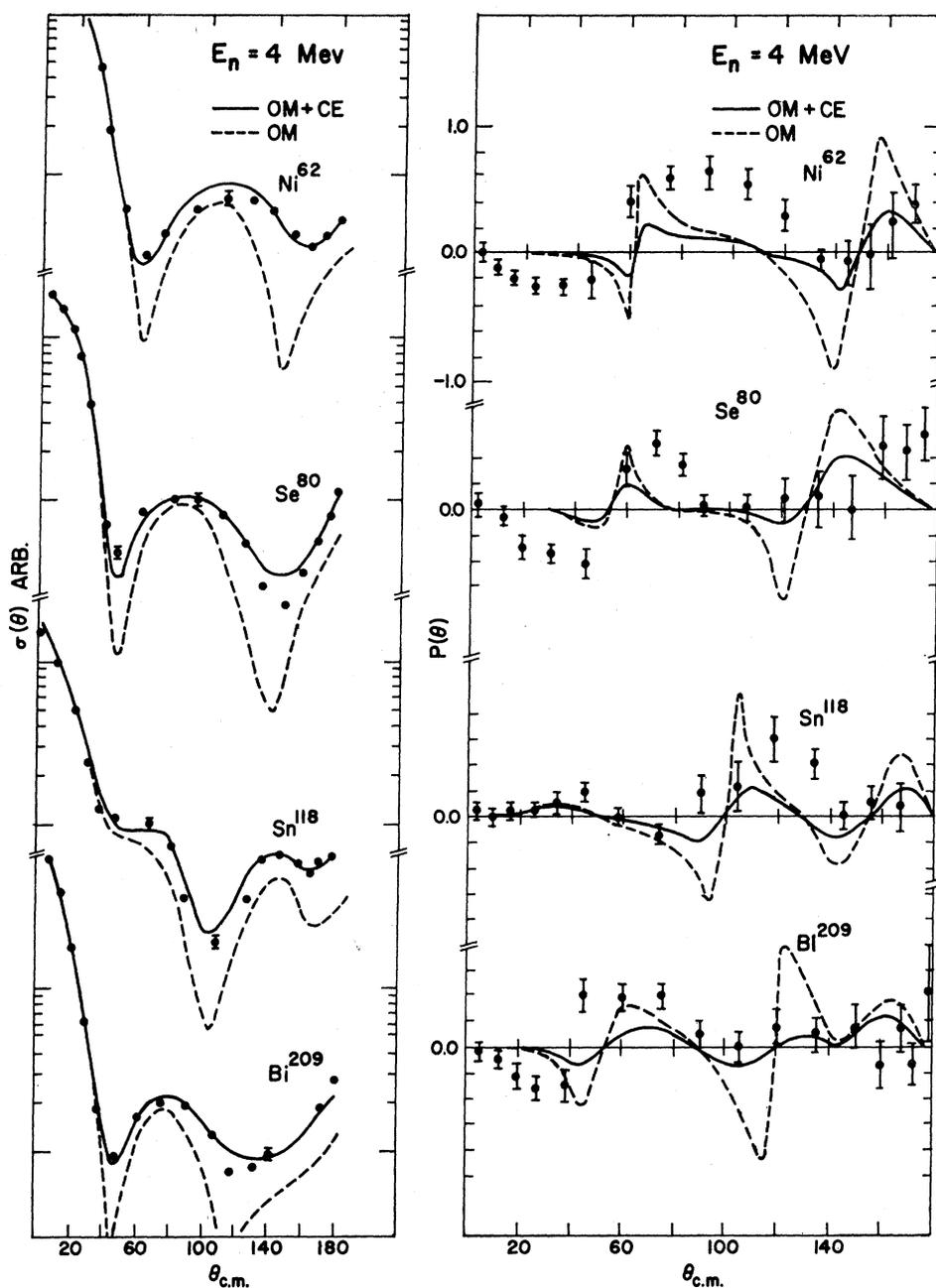
Fig. 17. Comparison of experimental cross-section and polarization data with the best-fit predictions for neutrons, $E_n=4$ MeV (Ref. 49).

neutron excess, $(N-Z)/A$. In the case of the proton parameters, which indicate a volume symmetry term, the data used in the analysis was primarily for nuclei with $(N-Z)/A<0.1$ and for energies $E>10$ MeV, while the neutron data, which was fitted slightly better with a surface term, weighted most heavily data with $(N-Z)/A>0.1$ and $E<15$ MeV. This suggests that the excess neutrons in the heavier nuclei are concentrated on the nuclear surface.

The spin-orbit potentials found here have a constant strength and geometry. The geometrical form factor shows either a smaller radius or a smaller diffuseness parameter than the real central potential. This is expected from Eqs. (10) and (11) which indicate that the difference of the msr of the real central and spin-orbit form factors is equal to $\langle r^2 \rangle_d$. Using the potential of Table I with $r_R = r_{so}$, yields results consistent with Eqs. (10) and (11) and a value for $\langle r^2 \rangle_d$ of 2.8 F^2, in agreement with the value of 2.25 ± 0.6 F^2 given by GPT. The highly localized nature of the spin-orbit interaction, as indicated by Eq. (11), is also reflected in the relative energy independence of V_{so}.
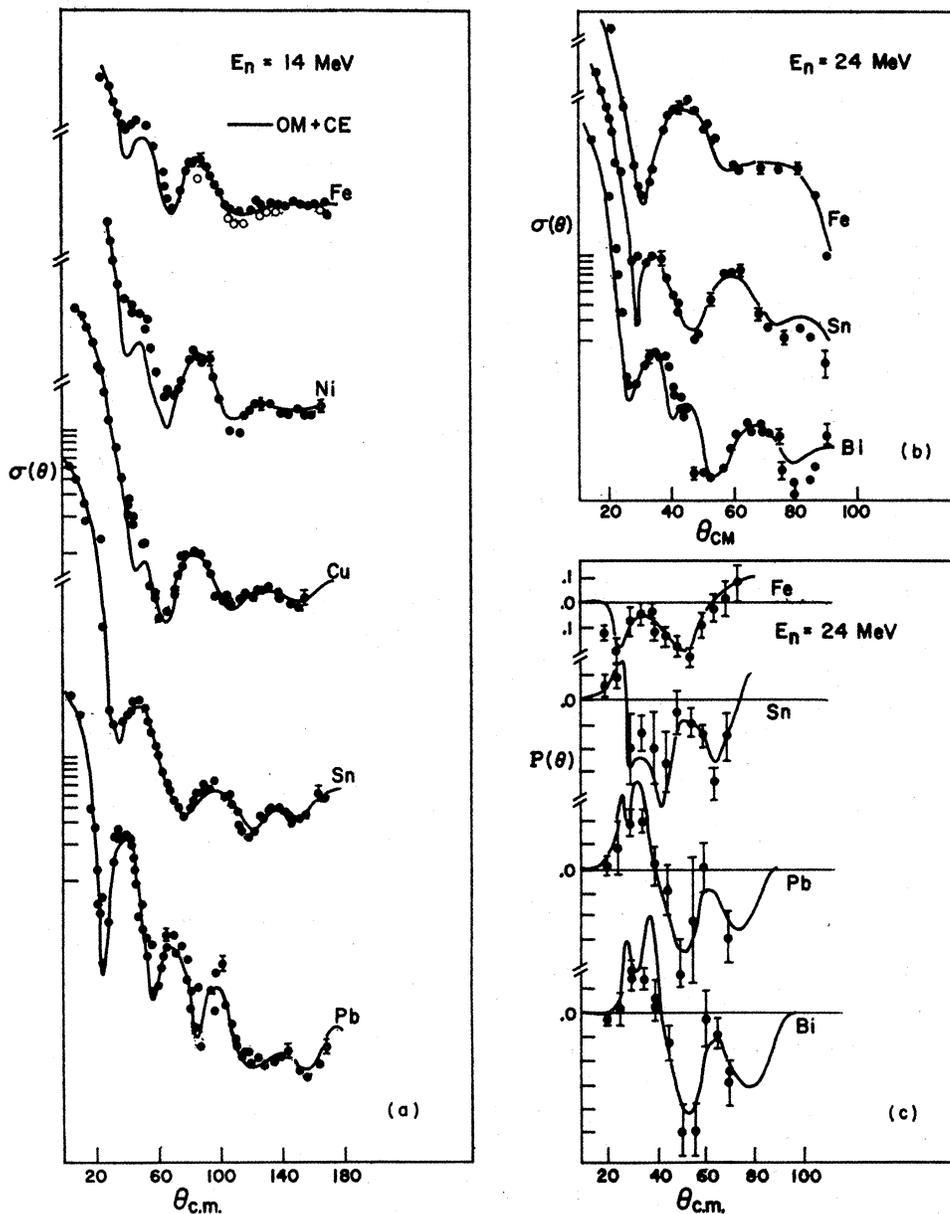
FIG. 18. Comparison of experimental cross-section and polarization data with the best-fit prediction for neutrons, $E_n = 14$ and 24 MeV. (a) Refs. 36, 37, (b) Ref. 38, and (c) Ref. 39.

VII. CONCLUSION

Although the primary motivation of the present OM analysis has been to find a suitable representation of available nucleon-nucleon elastic scattering data in the range $A > 40$, $E < 50$ MeV, the resulting OM parameters have been shown to be compatible with the physical processes involved and can be used with reasonable confidence to generate standard OM potentials in this region.

ACKNOWLEDGMENTS